IEEE Access
Multidisciplinary ⋮ Rapid Review ⋮ Open Access Journal

Received December 5, 2019, accepted December 30, 2019, date of publication February 6, 2020, date of current version February 19, 2020.

Digital Object Identifier 10.1109/ACCESS.2020.2972101

3D Printed Corrugated Plate Antennas With High Aperture Efficiency and High Gain at X-Band and Ka-Band

SHAKER ALKARAKI[1], (Member, IEEE), YUE GAO[2], (Senior Member, IEEE), SAMUEL STREMSDOERFER[3], EDOUARD GAYETS[3], AND CLIVE G. PARINI[1]

[1]School of Electronic Engineering and Computer Science, Queen Mary University of London, London E1 4NS, U.K.
[2]Institute for Communication, 5G innovation Centre, University of Surrey, Guildford GU2 7XH, U.K.
[3]Jet Metal Technologies, 69410 Champagne-au-Mont-d'Or, France

Corresponding author: Shaker Alkaraki (s.m.alkaraki@qmul.ac.uk)

This work was funded by the Engineering and Physical Sciences Research Council (EPSRC) in the United Kingdom under grant number EP/R00711X/1.

ABSTRACT A design criterion for a compact 3D printed high gain corrugated plate antenns that has high aperture efficiency and wide bandwidth is presented in this paper. The proposed design criterion is validated numerically and experimentally by fabricating 3D printed and Aluminium prototypes for X-band and Ka-band applications. The proposed antenna structure consists of two layers, where the electromagnetic energy (EM) is launched into a cavity that exists between both layers and the EM energy is coupled to the surface of the second layer. The second layer is the radiating structure which consists of three slots surrounded by a rectangular cavity and periodic corrugations that significantly improve the gain of the antennas. The 3D printed prototypes of the proposed antennas are fabricated and tested to validate the proposed design criterion, and their performance is compared to the Aluminium metallic counterparts. Using 3D printing technology, to fabricate the proposed antennas offer low cost and low weight alternatives to the Aluminium metallic prototypes. The measured results of the fabricated prototypes show high gain, high aperture efficiency, low side lobe level, and low cross polarization performance over a wide bandwidth.

INDEX TERMS 3D printing, aperture efficiency, slot antenna, corrugations, mm-wave, and metallization.

I. INTRODUCTION

Corrugated plate antennas have been widely investigated to deliver high gain performance at microwave frequencies, millimeter-wave and THz bands. These antennas typically consist of a central slot perforated into a metallic plate, where, the slot is surrounded by periodic corrugations that enhance the directivity of the antenna. The periodic corrugations have two main shapes which are straight corrugations (SC) as in [1]–[9] and cylindrical corrugations as known as ''Bull's Eye (BE)'' antennas [10]–[17]. One of the main advantages of these corrugated plate antennas is their ability of providing high gain performance, while keeping compact and low profile size. Hence, they found their way to be deployed for various applications at microwave frequencies [5], [6], [12], millimeter-wave and THz applications [2], [16], satellite communication [11], [12], and automotive radar communication [17]. Furthermore, one of the other advantages of the corrugated plate antennas that they have very high radiation efficiency, due to two main facts: the first is that the structures are typically fed using ultra reliable and efficient waveguide technology and the second is that the antenna structure consists of only metal, where the radiation efficiency of the antenna is boosted once the reflection coefficient is matched as the conduction losses of most metals such as Aluminum are very low. However, the main drawbacks of the SC and BE corrugated plate antennas that are their high cost of fabrication, low aperture efficiency and their narrow bandwidth.

Aperture efficiency (A_e) is the ratio of the effective aperture area of an antenna to the antenna's physical area. Generally, aperture antennas such as horn and reflectors have the highest aperture efficiency performance due to their high gain performance [18]–[20]. For example, horn antennas have an A_e range of 35% to 80% and optimum horn gain have an A_e of 50%, while reflectors have an A_e range of 50% to

The associate editor coordinating the review of this manuscript and approving it for publication was Yejun He.

80% [18]. However, high gain corrugated antennas have very compact size advantage compared to horn and reflectors, but they suffer from having low A_e performance due to their large aperture size as the corrugation's period is comparable to the operation wavelength. For example, the BE antennas in [11] and [17] have and $A_e$of less than 5 %, the BE antenna in [10] has an A_e of $\sim$ 6.5% and the improved and recent BE in [13] has an A_e of 32%. The antenna with SC in [1] has an A_e of $\sim$ 6% and the dual layer corrugated antenna with SC in [6] has an A_e of 18.5 %.

In this paper, we present a novel design criterion to overcome the low A_e disadvantage of corrugated antennas, while keeping compact and low profile advantage. The design criterion is able to deliver a design of compact corrugated antennas with high gain and high aperture efficiency performance at the same time. The design criterion is validated by fabricating and testing different 3D printed prototypes that operate at X-band and Ka-band. In addition, identical Aluminum prototypes are fabricated and tested to offer a performance comparison with the proposed 3D printed antennas. The proposed design criterion offers a significant improvement to the bandwidth of the antenna, in terms of -10 dB impedance bandwidth and 3 dB gain bandwidth. On top of that, the 3D printed antenna prototypes offer low cost and low weight alternatives, in comparison with the metallic prototypes.

II. ANTENNA STRUCTURE

Three 3D printed prototypes and two Aluminium prototypes are fabricated and tested to validate the proposed design criterion. The first two prototypes operate at X-band and they have the peak gain at 11.3 GHz, while other prototypes operate at Ka-band with the peak gain at 30 GHz. The Ka-band antenna is designed by scaling down the size of the X-band antenna and the schematics of the proposed antennas are shown in Figure.1 and Figure.2. The proposed antenna design consists of two layers stacked on top of each other as shown in Figure.1. The electromagnetic (EM) energy is launched from a standard rectangular waveguide into a rectangular cavity that exists between both layers on top of the bottom layer. WR90 waveguide with a dimensions of $a \times b = 22.86\ mm \times 10.16\ mm$ is used to feed the X-band antenna and the Ka-band antenna is fed using WR28 waveguide that has a dimensions of $a \times b = 7.11\ mm \times 3.56\ mm$. Each antenna has a dimensions of antenna width W and antenna length L and the cavity between both layers has a dimensions of cavity width Wc, cavity length Lc and cavity depth hc.

The thickness of the bottom layer is $t1$ and the thickness of the top layer is $t2$. The EM energy is coupled to the surface of the top layer (the radiating structure) from the cavity, which exists between both layers using the three slots that are perforated in the centre of the second layer as shown in Figure.2. The three slots have identical dimensions of slot length SL and slot width SW. Furthermore, a second rectangular cavity and periodic corrugations are designed on the surface of the top layer to boost the directivity of the antennas. The top layer cavity has a dimensions of $Wc1$, $Lc1$ and $hc1$. The dimensions of corrugations are: corrugation's width $k$and corrugation's depth $d$and the dimensions of the minor corrugation are$k1$and$d1$. The distance between the centre of the antenna and first corrugation is $r$and the corrugation's period is$p$. The detailed dimensions of the proposed antennas are provided in Table.1.

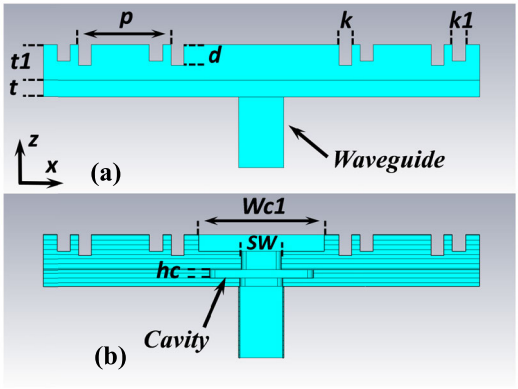

FIGURE 1. Schematic of the proposed antennas. (a) Side view and (b) cross section of side view.

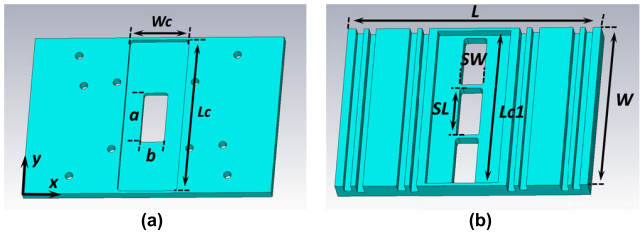

FIGURE 2. Schematic of the proposed antennas. (a) Perspective view of top view of first layer and (b) perspective view of top view of the second layer.

TABLE 1. The dimensions of the proposed antennas.

	(X-Band) $\lambda = 26.55\ mm$	(Ka-band) $\lambda = 10\ mm$
W	72 (2.7 λ)	31 (3.1λ)
L	102 (3.85 λ)	42(4.1λ)
Wc	24.8 (0.93 λ)	9.6(0.96λ)
Lc	70.5 (2.7 λ)	28 (2.8λ)
hc	0.5 (0.019 λ)	0.5 (0.05λ)
SL	21.5 (0.81 λ)	7 (0.7λ)
SW	9.5 (0.36 λ)	4(0.4λ)
$Wc1$	30 (1.13 λ)	11.4(1.14λ)
$Lc1$	70 (2.63 λ)	29.5(2.95λ)
$hc1$	4 (0.15 λ)	1.4(0.14λ)
$t1$	4 (0.15 λ)	2.5(0.25λ)
$t2$	8 (0.30 λ)	4.4(0.44λ)
p	22 (0.83 λ)	9.3(0.93λ)
d	5 (0.19 λ)	1.85(0.19λ)
$d1$	4 (0.15 λ)	1.2(0.12λ)
k	3 (0.11 λ)	1.3(0.13λ)
$k1$	3.2 (0.12 λ)	1.6(0.16λ)

III. ANALYSIS

A. OPERATION PRINCIPLES

Both of the proposed antennas have the same operation principles as the Ka-band antenna is designed by scaling down

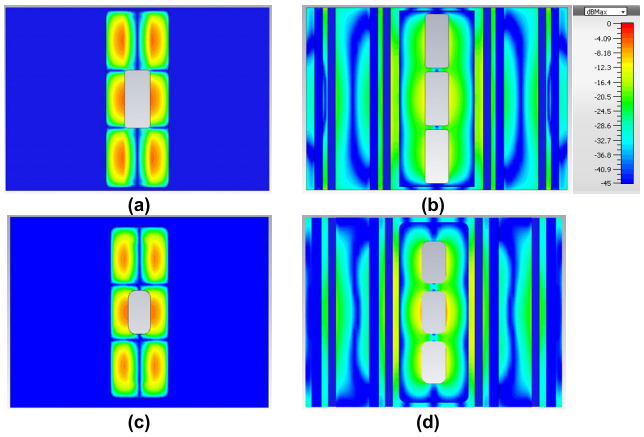

FIGURE 3. The electric field (E-field) distribution for the proposed antennas. (a) E-field in the cavity between both plates of the X-band antenna at 11.3 GHz, (b) E-field on the top layer at 11.3 GHz (c) E-field in the cavity of the Ka-band antenna at 30 GHz and (d) E-field on the top layer at 30 GHz.

the size of the X-band antenna. In both antennas, the EM energy is launched into the cavity between both layers using the waveguide as shown in Figure.3 (a) and (c). Then, the EM energy is coupled from the cavity to the second layer surface using the three slots. The slots radiate part of the coupled energy directly and the rest of the EM energy, which is polarized along the x-direction, is travelling and propagating at the antenna surface. Furthermore, the top layer rectangular cavity and the corrugations excite the travelling waves as shown in Figure.3 (b) and (d) resulting in a peak in the radiation once the dimensions of the cavity and the corrugations are optimized to provide radiation in the boresight direction at the desired frequency band as shown in Figure.4 and Figure.5. Therefore, the X-band antenna has a peak gain of 11.5 dBi due to the radiation from the slots only. Adding the two major set of corrugations on the second layer improves the gain 5.4 dBi to be 16.9 dBi. The gain of the antenna is further increased to 17.7 dBi after the addition of the minor corrugations and to 19.1 dBi, once the top layer cavity is added. The first optimization routine for the antenna dimensions to maximize the directivity of the antenna at the required band can be summarized as follows:

$$W \approx 3\lambda \tag{1}$$

$$d \approx \frac{\lambda}{5} \tag{2}$$

$$p + d \approx \lambda \tag{3}$$

$$Wc \approx Wc1 \approx \lambda \tag{4}$$

$$hc1 \approx \frac{\lambda}{7}\lambda \tag{5}$$

where λ is the operation wavelength.

The radiation from the slots and the top cavity is due to the strong excitation of TM_{320} mode in the cavity between both layers as shown in Figure.3 (a), (c) and Figure.4 (b). In more details, TM_{320} mode is strongly excited inside the

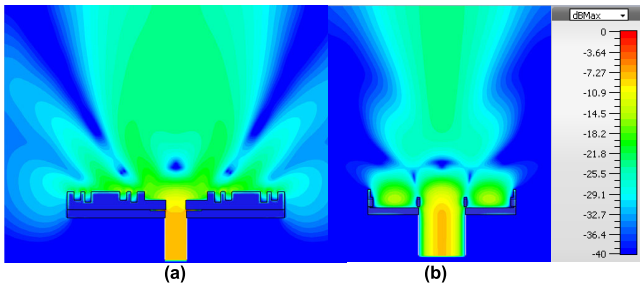

FIGURE 4. Power flow for the X-band antenna at 11.3 GHz. (a) (xz) cross section and (b) (yz) cross section.

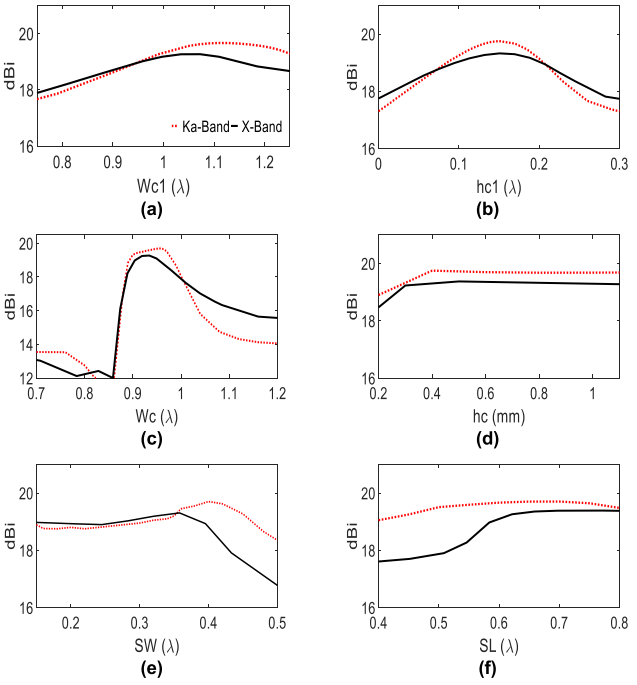

FIGURE 5. The relationship between dimensions of the antennas and the gain at 11.3 GHz and 30 GHz. (a) *Wc*1, (b) *hc*1, (c) *Wc*, (d) *hc*, (e) *SW* and (f) *SL*.

cavity as the electric field components E_z and magnetic field components H_x and H_y exists in the cavity with complete absense of E_y, E_x and $H_z = 0$. The cavity in the X-band antenna has a dimensions of $Wc \times Lc = 24.8\ mm \times 70.5\ mm$ which makes the cutoff frequency of TM_{32} mode inside the cavity is 13.8 GHz. However, the existance of the three slots on top of the cavity with dimensions of $SW = 9.5\ mm$, reduces the cutoff frequecny of the mode as it becomes possible to strongly start exciting the mode at 10.7$\sim$ 10.8 GHz as explained in equation 6 [24]. In fact, the three slots on top of the cavity enable the excitation of the mode at lower frequencies as the cavity looks practicallay wider to the electromagnatic waves as part of the mode is coupled from the cavity to the surface of the second layer using the top three slots. Hence, the excitation of the mode is possible once the width and length of the slots are optimized. This also explains why the antenna resonance frequency and directivity are sensitive to the slot dimensions SW, SL and to cavity

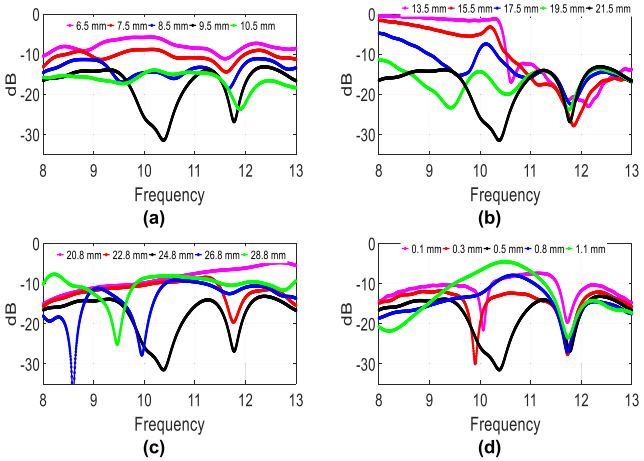

FIGURE 6. The effect of dimensions of the main antenna parameters on S_{11} performance of the X-band antenna. (a) *SW*, (b) *SL*, (c) *Wc* and (d) *hc*.

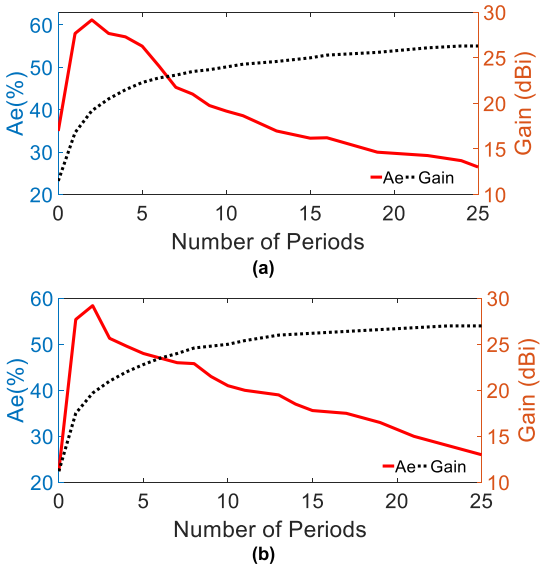

FIGURE 7. The relationship between number of periodic corrugations, aperture efficiency (A_e) and gain. (a) X-band antenna and (b) Ka-band antenna.

width Wc as shown in Figure.5 and Figure.6.

$$f_{c,mnp} = \frac{1}{2\pi\sqrt{\varepsilon\mu}}\sqrt{\left(\frac{m\pi}{Lc}\right)^2 + \left(\frac{n\pi}{Wc+Sw}\right)^2 + \left(\frac{p\pi}{h}\right)^2}, \quad m, n = 1, 2. \tag{6}$$

ε and μ are the permitivity and permeability of free space.

The excitation of the TM_{320} mode inside the cavities is also reflected in the gain performance of both antennas. For example, the X-band antenna has a simulated gain of 7.3 dBi at 10 GHz, it rises to 10.6 dBi at 10.4 GHz and to 14 dBi at 10.6 GHz. The gain of the antenna continues to rise to 15.4 dBi at 10.7 GHz and to 16.6 dBi at 10.8 GHz and to a peak of 19.1 dBi at 11.3 GHz. The Ka-band antenna gain and relationship with the excitation of TM_{320} mode follows the same trend as the X-band antenna. TM_{320} mode is excited inside the cavity as the cutoff frequency of the mode is reduced from 35.1 GHz to 27.3 GHz after the addition of the slots on the top layer as the combined width of the cavity and the slots is 10.6 *mm*. Hence, the Ka-band antenna has a gain of 13.2 dBi at 27.3 GHz and it rises to 16.1 dBi at 28 GHz.The gain of the Ka-band antenna contines to rise to 18.7 dBi at 29 GHz and to a peak of 19.7 dBi at 30 GHz.

The narrow periodic corrugations excite the travelling EM waves on the surface of the antenna as thoroughly analayzed and explained in [1]–[7]. In fact, *TE* mode is excited inside the narrow corrugations [20], [25] resulting in radiation in the boresight direction once the dimensions and the period of the corrugations are optimized. The relationhsip between the directivity of the major corrugations depth, width and period is studied in details in [6]. In fact, the field components inside the corrugations consists ofE_x, H_x, H_y and H_z with strong excitation of E_x and H_y and disappearance of E_z. Hence, the directivity of the antenna is sensitive to the dimensions of the depth of the corrugations D and the period of the corrugations $p$as the maximum directivity is achieved once the major corrugations depth is $\approx \frac{\lambda}{5}$ and when the period of the corrugations is $\approx 0.9\lambda$.

B. RELATIONSHIP BETWEEN THE APERTURE EFFICIENY, GAIN OF THE ANTENNAS AND NUMBER OF CORRUGATIONS

The relationship between the gain of the antennas and number of periodic corrugations is shown in Figure.7. The gain of the antennas is directly proportional to the number of periodic corrugations till reaching a saturation limit. For instance, the X-band antenna has a gain of 19.1 dBi with two set of corrugations and the gain rises to 20.5 dBi for 3 set of corrugations and to 22.3 dBi with 5 set of corrugations. The gain continues to rise to 24.2 dBi with 10 corrugations and it reaches a saturation limit of 26.3 dBi with 25 corrugations. However, the antenna has a simulted A_e of 58% with one set of corrugations and a peak A_e of 62% with two set of corrugations. The A_e drops to 58% with three corrugations and it steadily drops after that. For example, the antenna has an A_e of 55% with five corrugations, 40% with 10 corrugations, 33% with 15 corrugations and a minimum of 26% with 25 corrugations. The relationship between the gain and the number of periods of the Ka-band antenna follows the same trend as the X-band antenna with a difference that the Ka-band antenna has a relatively higher gain and lower A_e performacne as it has a sliglty larger electrical size. For example, the Ka-band antenna with two set of corrugations has a peak $A_e$of 57% and a peak gain of 19.7 dBi at 30 GHz and the antenna gain approaches saturation with 23 periods with 27 dBi and an A_e of 28%.

One of the main advantages of the proposed antenna structure in this paper is that the gain of the antenna is kept increasing even after adding more than 5 corrugations, unlike the single layer corrugated structures with straight corrugations presented in [1] and [6], where the gain of the antennas is almost reached the saturation limit with 5 periodic corrugations as the simulated saturation gain is 15.6 dBi in [1]

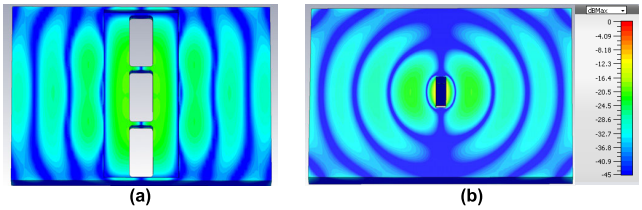

FIGURE 8. The Electric field on the surface of the antennas at 11.3 GHz. (a) the proposed X-band antenna with three slots and cavity and (b) antenna with a central slot.

and 14 dBi in [6]. This is due to the fact that the designed feeding mechanism of the proposed antennas in this paper couples an efficient planer-like wave to the surface of the antennas as shown in Figure.8 (a), therefore, the gain of the antenna continues to increase after adding more corrugations. However, the central slot in the case of the single layer corrugated antenna case in [1] and [6] couples a cylinderical-like wave to the surface of the antenna as shown in Figure.8 (b).

Hence, most of the coupled waves from the central slot are not excited after few corrugations and lost at the edges of the antenna. This explains why the Bull's Eye antenna proposed in litreture generally have higher gain and higher saturation number of periodic corrugations compared to the antennas with straight corrugations in [1] and [6] as the circular corrugations in the Bull's eye structure excite most of the coupled cylinderical waves on the antenna surface. However, the tradeoff of using the Bull's Eye structure fed using the cental slot to realize high gain performance remains the very large aperture size of the sturcture, resulting in low aperture efficiency perfomance as illustrated of all in the comparison of gain, size and A_e performance of all type of corrugated antenna structures available in literature in Table.4.

IV. FABRICATION METHOD

A. 3D PRINTING AND JET METAL METALLIZATION PROCESS

Each layer of the proposed antenna is 3D printed separately using Stratasys Objet30 Prime printer and with vero clear material. Objet30 prints a smooth structures with a maximum resolution of $100\mu m$ and a layer thickness of $16\mu m$. Then, the 3D printed plastic layers are metallized using Jet Metal (JMT) process described in Figure.9. The techniques which developed by Jet Metal technologies is a low cost metallization technique compared to electroless plating and it is used to plate a thin and very smooth silver layer (Ag) through spray coating using two spray guns at room temperature with ambient pressure. The fabrication process of the 3D printed antennas is summarized as follows: firstly, the 3D printed prototypes are washed by pressurized water to remove the support material that is used through the 3D printing process. Then, the holes of the screws were threaded using a conventional tap and die set that is typically used to thread screws in metallic structures. After that, the 3D printed prototypes are cleaned by Isopropyl Alcohol in order to remain grease

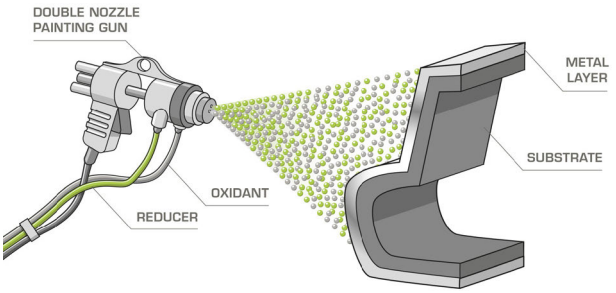

FIGURE 9. The principles of JMT process [22].

and stain. After cleaning, all layers were flame treated under high temperature in order to get a good wettability on the whole surface and to increase the adhesion of the silver coating. The resulting X-band prototypes before metallization are shown in Figure.10.(a) and (b). Then the X-band prototypes are metallized through spray coating thin silver layer. The prototypes are fixed on a holder with a rotation axis in order to get a homogeneous coating. A solution of activation was sprayed on the whole surface then rinsed and eventually silver plated by spraying the metallization solutions. Two spraying guns were used simultaneously during 13 minutes to reach a silver thickness of 2.5 μm which is thicker than the skin depth of Silver at 10 GHz and 30 GHz which is $\approx 0.7\mu m$ and $\approx 0.4\mu m$, respectively. The thickness of the silver layer can be simply controlled by controlling the spray time [21], [22].The plated silver layer with thickness of 2.5 μm has a measured surface resistance R_s of $9\sim 15m\Omega/\square$, resulting in conductivity of $2.7\times10^7 \sim 4.40\times10^7 s/m$. This contributes to negligible simulated conduction losses at X-band and Ka-band, in comparison to perfect electric conductor (PEC) and Aluminum which has a conductivity of $3.56\times10^7 s/m$ [23].

B. CONVENTIONAL MILLING

An identical prototype of the 3D printed antennas is fabricated using Aluminum using conventional computer numerical control (CNC) milling machine to provide a full comparison with the 3D printed antennas in terms of performance, cost of fabrication and weight. Each layer of each antenna is fabricated separately as the slots, cavity and corrugations are perforated on an Aluminum plate and the two plates are attached to each other using metallic screws. Then, coaxial to waveguide adapter is attached to the antennas as shown in Figure.11 (c). The detailed prototype of the Aluminum X-band antenna is shown in Figure.11 and the prototypes of the Ka-band Aluminum and the 3D printed metallized using JMT process are shown in Figure.12.

C. 3D PRINTING AND METALLIZATION USING ELECTROLUBE SILVER CONDUCTIVE PAINT

A second prototype of the Ka-band antenna is 3D printed and metallized using Electrolube silver conductive paint (SCP), due to the low performance of the 3D printed JMT antenna at Ka-band. The metallized prototype is shown in Figure.13. The paint is applied gently and manually using a fine brush

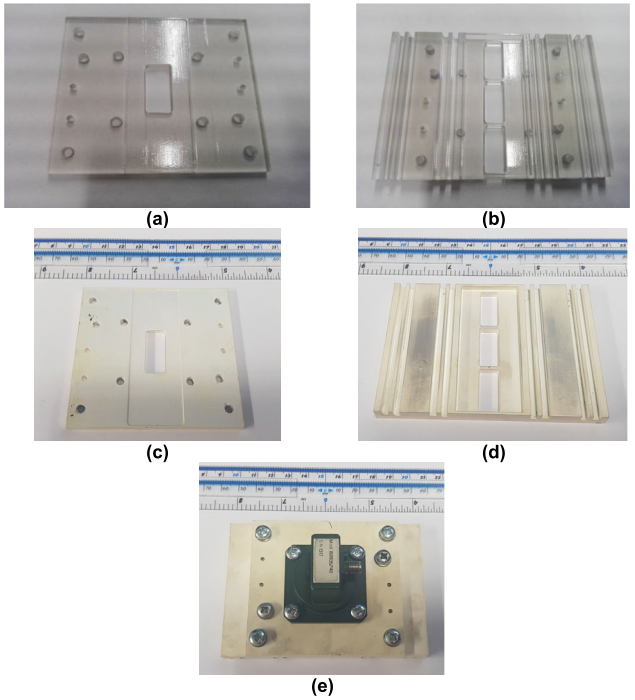

FIGURE 10. The 3D printed X-band antenna metallized using JMT process. (a) Top view of first layer before metallization, (b) top view of second layer before metallization, (c) top view of metallized first layer, (d) top view of metallized second layer and (e) bottom view of the assembled antenna with the WR90 coaxial to waveguide adapter.

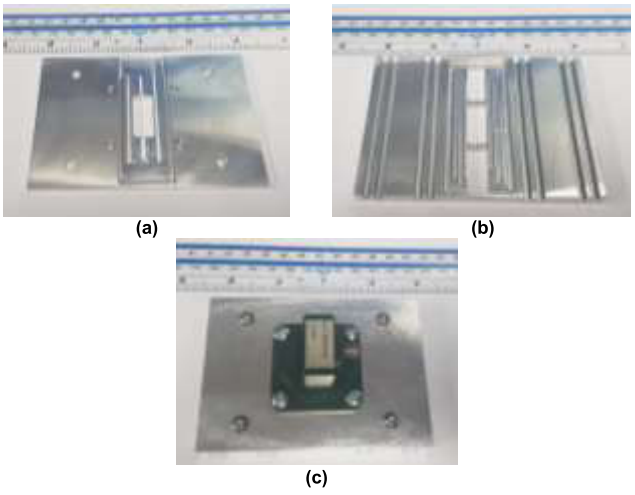

FIGURE 11. The prototype of Aluminium X-band antenna. (a) Top view of first layer, (b) top view of the second layer and (c) bottom view of the assembled antenna with WR90 coaxial to waveguide adapter.

paint on the surface of each layer of the antenna and left to dry for 10 minutes at room temperature. SCP is commercially available in bottles of either 3 grams, 25 grams or 50 grams. The paint has a 45% silver content mixed with solvent blend that has excellent adherence characteristics. One coat is applied on the surface of the antenna, except for the corrugations and the slots as more than one coat is required to guarantee full coverage of the paint, especially inside the corrugations, due to their small sizes. Using SCP as a metallization technique is simple and cheap as the 3D

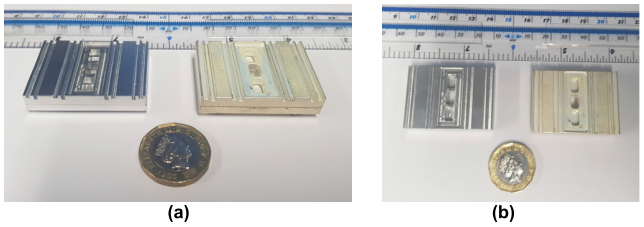

FIGURE 12. Perspective and top view of the Aluminum and 3D printed JMT Ka-band antennas. (a) Perspective view and (b) top view.

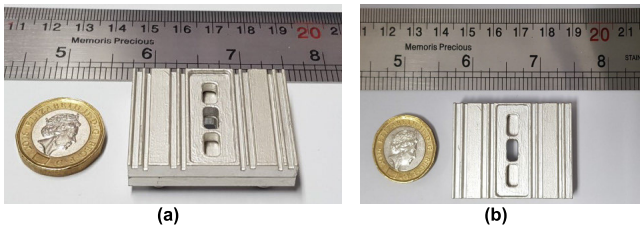

FIGURE 13. Perspective and top view of the Ka–band antenna metallized using Electrolube silver conductive paint (SCP). (a) Perspective view and (b) top view.

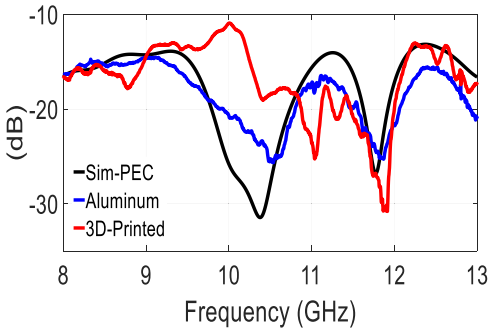

FIGURE 14. The simulated and measured S_{11} of the proposed X-band antennas.

printed prototypes do not need any special treatment before or after the metallization process.

V. RESULTS

A. X-BAND ANTENNA

Both X-band and Ka-band antennas are simulated using CST microwave studio and modelled as PEC. Furthermore, the reflection coefficient (S_{11}), gain and radiation patterns are measured. The S_{11} is measured using a vector network analyzer and the gain is measured using gain transfer method described in details in [26]. Both of the proposed Aluminum and 3D printed antennas have a measured -10 dB impedance bandwidth of 5 GHz covers the entire X-band as shown in Figure.14. Generally, a good agreement is found between the simulated and the measured S_{11} in the Aluminum antenna and the 3D printed antenna with some discrepancies.

The discrepencies between the measured and simulated S_{11} of both antennas are due to fabrication tolerences during the milling process in the Aluminum antenna case and the accuracy of the 3D printer in the the 3D printed antenna case. For example, the 3D printer prints with an accuracy of 0.1 *mm* which contributes to a fabrication uncertainity.

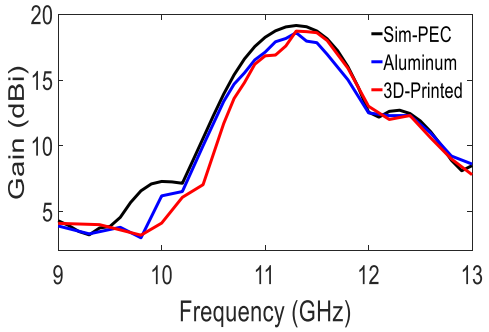

FIGURE 15. The simulated and the measured gain of the proposed Aluminum and 3D printed JMT antennas.

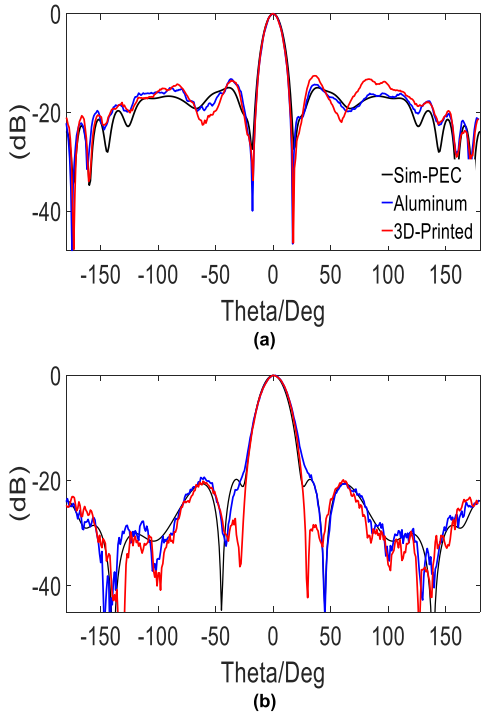

FIGURE 16. The simiualted and measured normalized radiation patterns at 11.3 GHz. (a) E-plane and (b) H-plane.

The measured gain and radiation patterns of the X-band antennas are shown in Figure.15 and Figure.16. The Figures show very good agreement between the simulated and measured results of both 3D printed JMT and Aluminum antennas. The simulated PEC antenna has a half power beamwidth (HPBW) of 20.6° in the H-Plane with side lobe level (SLL) of −19.8 dB and a HPBW of 14.4° and a SLL of −15.3 dB in the E-plane as shown in Figure.16.

The antenna radiates in the bresight direction over a bandwidth of 1.7 GHz (∼ 15%) range between 10.4 GHz and 12.1 GHz. The summary of the measured and simulated Figure of merits of each antenna are compared in Table.2. The PEC antenna has a simulated peak gain of 19.1 dBi at 11.3 GHz. The peak measured gain of the 3D printed antenna is 18.7 dBi which results in an aperture efficieny of 56.6% at 11.3 GHz. The measured peak gain of the Aluminum antenna is 18.6 dBi with an aperute efficieny of 55.4%.

TABLE 2. Comparison between the simualted and measured X-band antennas at 11.3 GHz.

	Gain (dBi)	*Ae (%)*	*HPBW E-Plane*	*HPBW H-Plane*	*SLL E-plane*	*SLL H-Plane*	*X-pol (dB)*
Simlated PEC	19.1	62	14.4°	20.6°	-15.3	-19.8	Na
3D printed measured	18.7	56.6	14.2°	20.9	-13.5	-20	-26
Aluminum measured	18.6	55.4	14°	21°	-14.2	-20	-28

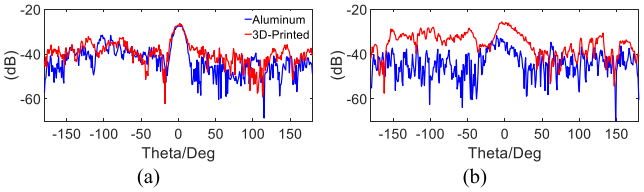

FIGURE 17. The measured cross polarisation (X-Pol) of both antennas. (a) E-plane and (b) H-plane.

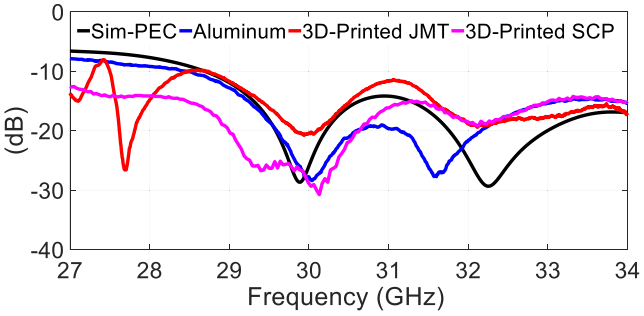

FIGURE 18. Simulated PEC and measured S_{11} of the 3D printed and Aluminum Ka-band antennas.

The 3D printed JMT antenna has a measured 3 dB gain bandwidth of 1.1 GHz and the Aluminum antenna has a 3 dB gain bandwidth of 1 GHz. This bandwidth corresponds to ∼ 10% and it is significantly wider than the bandwidth of other corrugated antennas available in literature [1]–[17].

B. KA-BAND ANTENNA

Simulated and measured S_{11} of the proposed Ka-band antennas is shown in Figure.18. A very good a greement is found between the simulated PEC and the measured results of both the 3D printed SCP antenna and the Aluminum antenna with less agreement with the measured 3D printed JMT anatenna. All propsoed Ka-band antennas have a wide −10 dB impedance bandwidth of more than 6 GHz, however, the radiation of the propsosed antennas in the boresight with low SLL performance is limited to a ≈ 4.1 GHz bandwidth, with a frequency range of 27.3 GHz to 31.4 GHz, reducing their boresight bandwidth to ∼ 13.7%. Furthermore, the 3D printed SCP antenna has a peak gain of 18.5 dBi at 30 GHz, compared to a measured peak gain of 18.9 dBi for the Aluminuim antenna and to 19.7 dBi for the simulated PEC gain. While, the 3D printed JMT antenna has only a

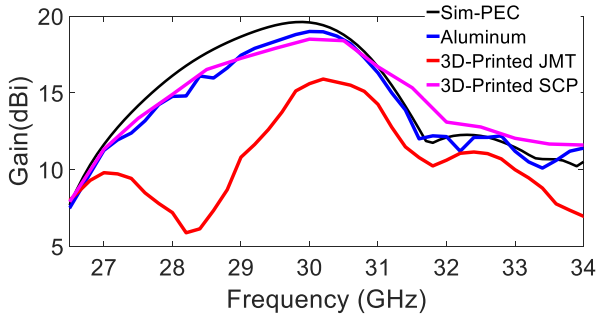

FIGURE 19. The simulated and measured gain of the proposed 3D printed and Aluminum antennas.

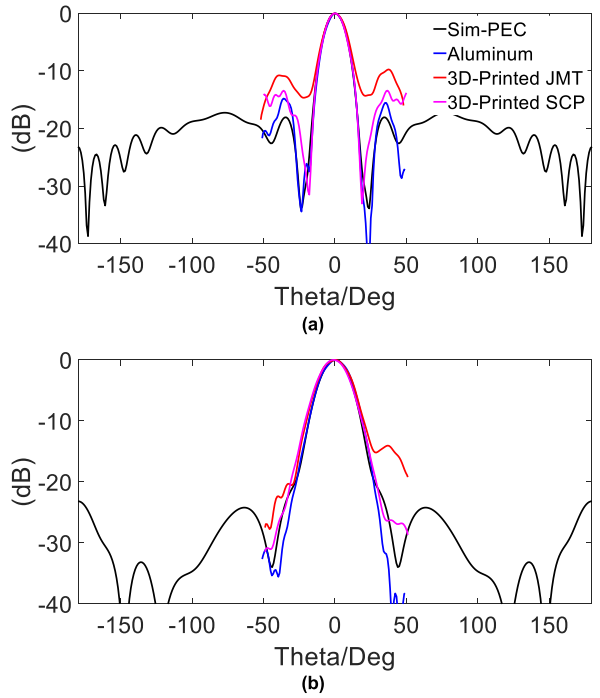

FIGURE 20. The simiualted and measured radiation patters at 30 GHz. (a) E-field and (b) H-field.

gain of 16.2 dBi at 30 GHz with gain losses of 3.5 dBi, in comparison with the simulated PEC antenna.

The 3 dB measured gain bandwidth of the 3D printed SCP antenna is 10.6% ranges between 28.2 GHz and 31.4 GHz, while it is 9% for the Aluminum antenna and 7% for the 3D printed JMT antenna. The gain of the proposed antennas are measured using gain transfer method described in [26] and far-field radiation patterns are calculated from the measurements of the antenna's near-field. The energy in the antenna's near-field region is measured and converted by the test system using Fourier transform into far-field measurement [27].

The measured patterns were only in the range of $40° \leq \mp\emptyset \leq 60°$, which is the maximum achievable angle range due to the limitation of planar near-field test system. A very good agreement is found between the results of the 3D printed antenna that is metallized using SCP and the Aluminium

TABLE 3. Comparison between the simualted and measured Ka-band antennas at 30 GHz (PEC is simulated and all other values are based on measured data).

	Gain (dBi)	*Ae (%)*	*HPBW E-Plane*	*HPBW H-Plane*	*SLL E-plane*	*SLL H-Plane*	*X-pol (dB)*
Simlated PEC	19.7	57	14.7°	20.4°	-16.3	-24	Na
3D printed JMT Mea	16.2	25.5	15.9°	21.9	-9.6	-14	-18
3D printed SCP Mea	18.5	43.3	14.2°	21.3°	-13.4	<-24	-24
Aluminum Measured	18.9	47.5	14.8°	21.1°	-14.5	<-24	-29

antenna, in comparsion with the simulated results as shown in Figure. 19 and Figure. 20 and summarized in Table.3. For example, the 3D printed SCP antenna has a peak gain of 18.5 dBi with HPBW of 14.2° at 30 GHz in the E-plane and 21.3° in the H-plane with good agreement with the Aluminum antenna which has a peak gain of 18.9 dBi and HPBW of 14.8° at 30 GHz in the E-plane and 21.1° in the H-plane. However, a less agreement is found between the 3D printed JMT antenna and other antennas as the the 3D printed JMT antenna has significanty lower gain performance and higher SLL compared to simulated PEC antenna, 3D printed SCP antenna and Aluminum antenna at Ka-band as compreheni-sively compared in Table.3.

The discrepancies between the measured and simulated antennas are due to fabrication tolerences of milling process in the Aluminum antenna case, and due to the accuracy of the 3D printer which corrosponds to $\lambda/100$ at 30 GHz. This contributes to a fabrication tolerences that has a minor effect on the performance of the Aluminuim and 3D printed antenna as the used 3D printer is with high resolution. However, the major reasons which deteriorate the performance of the 3D printed antennas are the existance of the air gap between both layers in the case of the 3D printed JMT antenna and the lower conductivity of the SCP paint and the non-uniform paint thickness in case of the 3D printed SCP 3D printed antenna.

A small flexure and bend is observed in the first layer of the plastic 3D printed JMT ka-band antenna. This flexure is due to exposure to high heat during the flamming process which has been implemented to improve the wettability of the surface of the material prior to applying JMT silver paint on the plastic surface during the metallization process. This flexure and bend causes an air gap between both layers that has significantly detoriorated the gain and the radiation pattern performance of the antenna at Ka-band as the antenna is more sensitive to fabrication tolerances, unlike the X-band 3D printed JMT antenna which did not have this problem as the first layer of the 3D printed JMT antenna is thicker, and hence it is less sensitive to heat treatment.

However, the discrepencies between the 3D printed SCP antenna and the Aluminium and simulated PEC antenna is

TABLE 4. Performance comparison between different corrugated plate antennas, horns and the proposed antennas.

Antenna	*Dimensions*	*Frequency (GHz)*	*Bandwidth 3dB-Gain (%)*	*Bandwidth (-10 dB) (%)*	*Gain (dBi)*	*A_e (%)*	*X-pol (dB)*	*SLL (dB)*
3D printed – X-band - this work	$3.85\lambda \times 2.7\lambda \times 0.45\lambda$	11.3	9.7	38	18.7	56.6	-26	-13.5
Aluminum – X-band - this work	$3.85\lambda \times 2.7\lambda \times 0.45\lambda$	11.3	8.9	38	18.6	55.4	-28	-14.2
3D printed JMT – Ka-band- this work	$4.1\lambda \times 3.1\lambda \times 0.69\lambda$	30	7	> 30	16.2	25.5	-18	-9.6
3D printed SCP – Ka-band- this work	$4.1\lambda \times 3.1\lambda \times 0.69\lambda$	30	10.6	> 30	18.5	43.3	-24	-13.4
Aluminum – Ka-band- this work	$4.1\lambda \times 3.1\lambda \times 0.69\lambda$	30	9	> 30	18.9	47.5	-29	-14.5
Bull's Eye 1 [12]	$\approx 20\lambda \times 20\lambda \times 0.5\lambda$	60	NA	≈8.4	19.7	≈2	NA	-14
Bull's Eye 2 [14]	$\approx 5\lambda \times 5\lambda \times 0.5\lambda$	60	2.78	16	20.2	32	-15	-13.2
Bull's Eye 3 [11]	$\approx 15\lambda \times 15\lambda \times 0.7\lambda$	16	NA	≈ 5	21	≈7	-25	-15
Straight corrugations [6]	$3.8\lambda \times 4.9\lambda \times 0.63\lambda$	11.3	≈10	≈23	16.3	18.5	-35	-15
Straight corrugations [1]	$\approx 17.6\lambda \times 4.4\lambda \times 0.66\lambda$	16.5	NA	≈ 7	18	≈ 6	NA	$\approx$ -10
Straight corrugations [10]	$\approx 3.2\lambda \times 2\lambda \times 0.75\lambda$	14.6	NA	≈ 4.5	15.9	≈ 49	NA	-10.9
Straight corrugations [21]	$17.3\lambda \times 1.05\lambda \times 0.61\lambda$	28.6	NA	9.8	16.7	18.8	NA	NA
Straight corrugations [21]	$1.9\lambda \times 1.05\lambda \times 0.61\lambda$	28.5	NA	9.8	12.9	78	-34	-9.5
Ka-band-**horn** - SAR-1725-28-S2	$2.74\lambda \times 2.2\lambda \times 3.8\lambda$	30	≈ 30	≈45	≈16.5	58	NA	-11
Ka-band-**horn** - SAR-2013-28-S2	$4.24\lambda \times 3.35\lambda \times 5.84\lambda$	30	≈ 30	≈45	≈19.4	48.5	NA	-10
X-band- **horn** - PE9856-20	$3.54\lambda \times 4.79\lambda \times 9.64\lambda$	11.3	≈ 30	≈40	20	47	NA	NA
Horn - SAK-AR073123-96-C2	$3.9\lambda \times 3.58\lambda \times 7.4\lambda$	11.3	≈ 30	≈45	≈19.3	49	NA	NA

TABLE 5. Weight comparison between the proposed antennas and horn antennas.

Antenna	*Weight (grams)*
Aluminum X-band	195
3D printed X-band	79
Aluminum Ka-band	21
3D printed Ka-band	9.8
X-band- Horn- PE9856-20	340
X-band - Horn- SAK-AR073123-96-C2	209
Ka-band-Horn - SAR-1725-28-S2	12
Ka-band-Horn - SAR-2013-28-S2	17

due to combination of reasons. The first is tolerances of the 3D printer as dicussed previously and the second is the non-uniform thickness of the paint across the antenna surface, especially inside the corrugations, while the third reason is the lower conductivity of the used SCP paint, in comparison to Aluminium and PEC. In more details, the propsoed SCP 3D printed antenna is painted manually using a paint brush, where more than one coat is needed to fully cover the area inside the small corrugations and the slots which produces a non-uniform thickness of the paint, especailly inside the corrugations. This causes the dimensions of the corrugations to be smaller in comparison to the original dimensions in which causes deterioration in the performance of the S_{11}, raidation patterns, SLL and gain. For example, the meausured gain as shown in Figure 19 shows that the proposed SCP 3D printed antenna has better gain performance than the PEC antenna at higher frequencies as the corrugations are effectively smaller than the PEC antenna due to paint thickness. The thickness of each coat is measured to be between $\approx 30\mu m$and $45\mu m$. Furthermore, SCP paint has 45% silver content mixed with solvent blend that helps the silver to excellently adhere on the plastic surfaces. Hence, the paint conductiviy (σ) is lower than Aluminium and pure silver and it can be calculated from the measurement of it sheet resistance R_s after applying the paint using the following formula:

$$R_s = \frac{\rho}{t} \tag{7}$$

Where, $R_s$is measured in ohm per squar ($\Omega/\square$), ρ is the resistivty (Ω), t is the thickness of the paint, and $\sigma = \frac{1}{\rho} = S.m^{-1}$ [23].

For example, the proposed conductivity of SCP ranges between $\approx 0.82 \times 10^6$to 2.2×10^6, when the paint thickness ranges between 30 μm and 45 μm as the measured $R_s$using four point probe on the antenna surface ranges between 13 $m\Omega/\square$ and 27 $m\Omega/\square$. Hence, the approximation of antenna losses due to the variation of conductivity of the paint at 30 GHz ranges between 0.5 dB and 0.7 dB as the simulated results shows in Figure. 21 and the rest of gain losses which is $\approx$ 0.5 dB are due to non- uniform paint thickness and 3D printing tolerances. Finally, surface roughness of the 3D printed antenna is unlikely responsible for any gain losses as Objet30 prime prints prototypes with smooth surface that have very low surface roughness. For example, the measured root mean square (RMS) surface roughness of the prototypes is less than 1.82 μm for the 3D printed prototypes metallized using JMT process and it is less than 4.62 μm for the

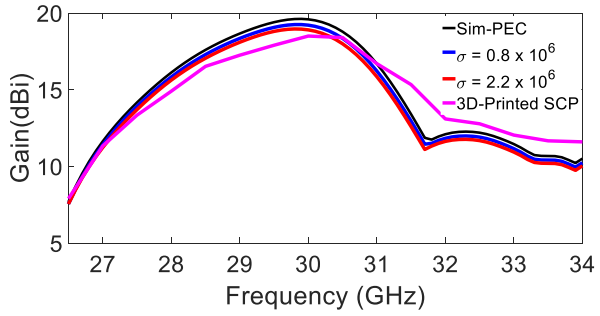

FIGURE 21. The effect of conductivity on the gain of the propsoed SCP 3D printed antenna (σ values are in $S.m^{-1}$).

prototypes metallized using SCP paint. This is much less than the surface roughness RMS value of 25.9 μm, which has contributed to no losses in the horn gain at 15 GHz as discussed in [28].

Finally, the figure of merits of the proposed Aluminum and 3D printed antennas are compared in details with other similar corrugated antennas and standard gain horns as summarized in Table.4. All of the proposed antennas in this paper have significantly wider -10 dB impedance bandwidth and 3 dB gain bandwidth, in comparsion to all other antennas in [1]–[18], [21].

Furthermore, the X-band and Ka-band 3D printed antennas as well as the Aluminum antennas have much higher aperture efficiecny performance than all other corrugated antennas proposed in litreture, except for the single layer Ka-band corrugated antenna propsoed in [21] which has an A_e of 78% and a peak gain of 12.9 dBi at 28.5 GHz with one set of corrugations. However, the antenna in [21] suffers from having low gain performance in comparison to the antennas proposed in this paper as its saturation peak gain is 16.3 dBi once extra corrugations are added which lower its A_e to 18.8% [21]. Moreover, the proposed antennas have high gain and high aperture efficiency performance comparable and in some cases higher than X-band and Ka-band standard gain horn antennas as shown in Table.4. For example, both of the proposed X-band antennas have higher aperture efficincy at 11.3 GHz than the horns with slightly lower gain performance. Besides, the proposed antennas have much more compact height than the horns, as PE9856-20 horn with height of 9.64λ is 21 times higher than the proposed X-band antennas, and the SAK-AR073123-96-C2 horn is 16 times higher than the proposed X-band antennas. In addition, SAR-2013-28-S2 horn is 8.4 times higher than the proposed Ka-band antennas, while SAR-1725-28-S2 horn is 5.5 times higher than the proposed Ka-band antennas. Furthermore, the proposed antennas exhibit lower weight characteristics, especially for the 3D printed antennas over the horns as compared in Table.5. However, the only superiority of the horns over the proposed antennas that they have stable gain and radiation pattern performance over very wide bandwidth covers the entire X-band and Ka-band. Finally, the proposed 3D printed antennas have much lower cost of fabrication. For example, the cost of the material used to 3D print the X-band 3D printed antenna is less than 45 USD and it less than 8 USD for the Ka-band 3D printed antenna. Combining the cost of 3D printing with the cost of the material used in the metallization process which is few dollars in both cases reduces the overall cost of the proposed 3D printed antennas, in comparison to the Aluminum prototypes and to the horns as they have significantly much higher cost of fabrication.

VI. CONCLUSION

A design criterion for high gain 3D printed corrugated plate antennas with high aperture efficiency is demonstrated in the paper. The proposed antenna design consists of two layers where the first layer is used to feed the second layer which is the radiating structure. The second layer consists of three radiating slots surrounded by rectangular cavity and periodic corrugations. The slots are used to couple the electromagnetic energy from a cavity that exists on top of the first layer to the second layer surface.

The proposed design criterion provides antennas with high aperture efficiency, wide bandwidth and high gain performance due to the combined radiation from the slots, cavity and corrugations. Furthermore, the proposed design criterion is validated by fabricating several prototypes at X-band and Ka-band. For example, the proposed X-band antennas have wide bandwidth that covers the entire X-band with a peak measured gain of higher than 18 dBi at 11.3 GHz, while the Ka-band antennas have peak measured gain of 18.5 dBi at 30 GHz, resulting in high aperture efficiency performance. This offers the proposed 3D printed antennas to be low cost solution with an advantages of providing high gain with high aperture efficiency performance, while keeping compact and low profile size.

REFERENCES

[1] M. Diaz, I. Campillo, J. Dolado, J. Rodriguez-Seco, E. Perea, F. Falcone, and M. Ayza, "Dual-band low-profile corrugated feeder antenna," *IEEE Trans. Antennas Propag.*, vol. 54, no. 2, pp. 340–350, Feb. 2006.

[2] M. Beruete, U. Beaskoetxea, M. Zehar, A. Agrawal, S. Liu, K. Blary, A. Chahadih, X.-L. Han, M. Navarro-Cia, D. E. Salinas, A. Nahata, T. Akalin, and M. S. Ayza, "Terahertz corrugated and bull's-eye antennas," *IEEE Trans. THz Sci. Technol.*, vol. 3, no. 6, pp. 740–747, Nov. 2013.

[3] C. Huang, Z. Zhao, and X. Luo, "The rectangular waveguide board wall slot array antenna integrated with one dimensional subwavelength periodic corrugated grooves and artificially soft surface structure," *J Infr. Milli Terahz Waves*, vol. 30, no. 4, pp. 357–366, Apr. 2009.

[4] X. Gao, S. M. Li, W. P. Cao, Q. Cheng, H. F. Ma, and T. J. Cui, "A highly directive slot antenna with sidewall corrugated structure," *IEEE Antennas Wireless Propag. Lett.*, vol. 12, pp. 1582–1585, 2013.

[5] S. Alkaraki, Y. Gao, and C. Parini, "Dual-layer corrugated plate antenna," *IEEE Antennas Wireless Propag. Lett.*, vol. 16, pp. 2086–2089, 2017.

[6] S. Alkaraki, A. S. Andy, Y. Gao, K.-F. Tong, Z. Ying, R. Donnan, and C. Parini, "Compact and low-cost 3-D printed antennas metalized using spray-coating technology for 5G mm-wave communication systems," *IEEE Antennas Wireless Propag. Lett.*, vol. 17, no. 11, pp. 2051–2055, Nov. 2018, doi: 10.1109/lawp.2018.2848912.
[7] C. Huang, Z. Zhao, Q. Feng, and X. Luo, "Suppression of grating lobes from a corrugated 2×2 slot antenna array with element spacing beyond a wavelength," *IET Microw. Antennas Propag.*, vol. 5, no. 13, pp. 1607–1612, Oct. 2011.
[8] C. Huang, Z. Zhao, Q. Feng, and X. Luo, "A high-gain antenna consisting of two slot elements with a space larger than a wavelength," *IEEE Antennas Wireless Propag. Lett.*, vol. 9, pp. 159–162, 2010.
[9] M. Beruete, I. Campillo, J. S. Dolado, J. E. Rodriguez-Seco, E. Perea, F. Falcone, and M. Sorolla, "Very low-profile 'bull's eye' feeder antenna," *IEEE Antennas Wireless Propag. Lett.*, vol. 4, pp. 365–368, 2005.
[10] C. J. Vourch and T. D. Drysdale, "V-band 'bull's eye' antenna for cubesat applications," *IEEE Antennas Wireless Propag. Lett.*, vol. 13, pp. 1092–1095, 2014.
[11] C. J. Vourch and T. D. Drysdale, "V-band Bull's eye antenna for multiple discretely steerable beams," *IET Microw., Antennas Propag.*, vol. 10, no. 3, pp. 318–325, Feb. 2016.
[12] U. Beaskoetxea and M. Beruete, "High aperture efficiency wide corrugations bull's-eye antenna working at 60 GHz," *IEEE Trans. Antennas Propag.*, vol. 65, no. 6, pp. 3226–3230, Jun. 2017.
[13] S. Alkaraki, Y. Gao, C. Parini, M. Navarro-Cia, and M. Bernete, "Linearly and circularly polarised bull's eye antenna," in *Proc. Loughborough Antennas Propag. Conf. (LAPC)*, Loughborough, U.K., Nov. 2016, pp. 1–3.
[14] S. Alkaraki, Z. Hu, and Y. Gao, "High gain and steerable bull's eye millimetre wave antenna," in *Proc. IEEE Int. Symp. Antennas Propag. USNC/URSI Nat. Radio Sci. Meeting*, Vancouver, BC, Canada, Jul. 2015, pp. 2041–2042.
[15] U. Beaskoetxea, S. Maci, M. Navarro-Cia, and M. Beruete, "3-D-printed 96 GHz bull's-eye antenna with off-axis beaming," *IEEE Trans. Antennas Propag.*, vol. 65, no. 1, pp. 17–25, Jan. 2017.
[16] U. Beaskoetxea, V. Pacheco-Pena, B. Orazbayev, T. Akalin, S. Maci, M. Navarro-Cia, and M. Beruete, "77-GHz high-gain bull's-eye antenna with sinusoidal profile," *IEEE Antennas Wireless Propag. Lett.*, vol. 14, pp. 205–208, 2015.
[17] C. A. Balanis, "Aperture antennas," in *Antenna Theory*, 3rd ed. Hoboken, NJ, USA: Wiley, 2005, ch. 12, sec. 5.3, p. 682.
[18] K. F. Warnick and B. D. Jeffs, "Gain and aperture efficiency for a reflector antenna with an array feed," *IEEE Antennas Wireless Propag. Lett.*, vol. 5, pp. 499–502, 2006.
[19] S. Alkaraki, Y. Gao, and C. Parini, "High aperture efficient slot antenna surrounded by the cavity and narrow corrugations at Ka-band and Ku-band," *IET Microw., Antennas Propag.*, vol. 12, no. 12, pp. 1926–1931, Oct. 2018.
[20] G. Stremsdoerfer, *Techniques de L'ingénieur, JetMetal: Procédé Innovant de Dépôts Métalliques ou D'alliages*, document IN204, Oct. 2012.
[21] A. Jammes, M. Petisme, and K. Staelens, "Metaliztion and selevtive metalization of silver using spraying," *Surf. Coating Technol.*, vol. 322, pp. 560–563, Dec. 2017.
[22] S. Alkaraki, Y. Gao, M. O. Munoz Torrico, S. Stremsdoerfer, E. Gayets, and C. Parini, "Performance comparison of simple and low cost metallization techniques for 3D printed antennas at 10 GHz and 30 GHz," *IEEE Access*, vol. 6, pp. 64261–64269, 2018.
[23] M. D. Pozar, "Tansmission line and waveguides," in *Microawave Engineering*, 3rd ed. Danvers, MA, USA: Wiley, 2005, ch. 3, sec. 3.3, p. 112.
[24] D. Y. Na, K.-Y. Jung, and Y. B. Park, "Transmission through an annular aperture surrounded with corrugations in a PEC plane," *IEEE Antennas Wireless Propag. Lett.*, vol. 14, pp. 179–182, 2015.
[25] C. A. Balanis, "Antenna measurement," in *Antenna Theory*, vol. 2, 3rd ed. Hoboken, NJ, USA: Wiley, 2005, ch. 17, sec. 4, pp. 1033–1034.
[26] S. M. Gregson and C. J. Parini, *IET Electromagnetic Waves Series, Principles of Planar Near-Field Antenna Measurements*, vol. 53. London, U.K.: Institution of Engineering and Technology, 2007.
[27] C. Garcia, H. Tsang, J. Barton, and R. Rumpf, "Effects of extreme surface roughness on 3D printed horn antenna," *Electron. Lett.*, vol. 49, no. 12, pp. 734–736, Jun. 2013.

SHAKER ALKARAKI (Member, IEEE) received the B.Sc. degree (Hons.) in communication engineering from International Islamic Malaysia IIUM, in 2011, the M.Sc. degree (Hons.) from The University of Manchester (UoM), in 2013, and the Ph.D. degree in electronic engineering from the Queen Mary University of London (QMUL), in 2019. He is currently a Postdoctoral Researcher with the Antennas and Electromagnetics Group, QMUL. His research interests include mm-wave antennas, mm-wave phased arrays, 3D printed antennas, metallization techniques, 5G antennas and systems, large scale arrays, high gain antennas, MIMO, leaky waves, and reconfigurable liquid metal antennas. He was a recipient of IIUM B.Sc. Scholarship, UoM M.Sc. Scholarship, and QMUL Ph.D. Scholarship.

YUE GAO (Senior Member, IEEE) received the Ph.D. degree from the Queen Mary University of London (QMUL), U.K., in 2007. He was a Lecturer, a Senior Lecturer, and a Reader in antennas and signal processing with QMUL. He is currently a Professor and a Chair in wireless communications with the University of Surrey. He is leading a team developing fundamental research into practice in the interdisciplinary area of smart antennas, signal processing, spectrum sharing, millimetre-wave, and the Internet of Things technologies in mobile and satellite systems. He has published more than 180 peer-reviewed journal and conference papers, 2 patents, 1 book, and 5 book chapters.

He is an Engineering and Physical Sciences Research Council Fellow from 2018 to 2023. He was a co-recipient of the EU Horizon Prize Award on Collaborative Spectrum Sharing in 2016. He served as the Signal Processing for Communications Symposium Co-Chair for IEEE ICCC 2016, the Publicity Co-Chair for the IEEE GLOBECOM 2016, the Cognitive Radio Symposium Co-Chair for the IEEE GLOBECOM 2017, and the General Chair for the IEEE WoWMoM and iWEM 2017. He is the Chair of the IEEE Technical Committee on Cognitive Networks and the IEEE Distinguished Lecturer of the Vehicular Technology Society. He is an Editor for the IEEE Internet of Things Journal, the IEEE Transactions on Vehicular Technology, and the IEEE Transactions on Cognitive Networks.

SAMUEL STREMSDOERFER received the M.Sc. degree in applied chemistry from the Ecole supérieure de Chimie Physique Electronique, in 2004, and the M.Sc. degree in management from the Emlyon Business School, Lyon, France, in 2007. He was a Graduate Student with the Ecole Supérieure de Chimie Physique Electronique, from 2003 to 2005. He is currently a Founder and a CEO of Jet Metal Technologies, Lyon, since 2005. He is also an experienced chief executive officer working in the mechanical and industrial engineering industry. Skilled in research and development (R&D), chemistry, innovation management, materials science, and chemical engineering.

EDOUARD GAYETS received the bachelor's degree in science of matter from Université Jean Monnet Saint-Etienne, in 2002, and the M.Sc. degree in material chemistry from Université Claude Bernard Lyon 1, in 2004. He worked as a Trainee in chemical engineering with Thales Systems Aeroportes SAS, in 2005. He has been a Senior Research and Development (R&D) Engineer with Jet Metal technologies (JMT), Lyon, France, since 2007. He has worked extensively with JMT Team on developing solutions of metal coatings for decoration, conductivity, electromagnetic shielding, surface hardness, corrosion protection, and other functionalities.

CLIVE G. PARINI received the B.Sc. (Eng.) and Ph.D. degrees from the Queen Mary University of London, London, U.K., in 1973 and 1976, respectively. He joined the Queen Mary University of London as a Lecturer in 1977, promoted to a Reader in 1990 and to a Professor in 1999, where he is currently a Professor of antenna engineering and the Head of the Antenna and Electromagnetics Research Group. He has published more than 450 articles on research topics, including array mutual coupling, array beam forming, antenna metrology, microstrip antennas, millimeterwave compact antenna test ranges, millimeterwave integrated antennas, metamaterials, and on-body communications. He has coauthored two books, i.e., *Principles of Planar Near-Field Antenna Measurements* (IET, 2008) and *Theory and Practice of Modern Antenna Range Measurements*, (IET, 2014) in the Electromagnetic Wave Series.

He is a Fellow of the IET. He was a member of the Editorial Board until January 2015 and an Honorary Editor for the IET *Journal of Microwaves, Antennas and Propagation*. In 2009, he was elected as a Fellow of the Royal Academy of Engineering. He is a Chartered Engineer and a Fellow of the IET. He was the Chairman of the IET Antennas and Propagation Professional Network Executive Team.